Focusing of surface-acoustic-wave fields on (100) GaAs surfaces

M. M. de Lima, Jr.,[a] F. Alsina, W. Seidel, and P. V. Santos
Paul-Drude-Institut für Festkörperelektronik, Hausvogteiplatz 5–7, 10117 Berlin, Germany

(Received 3 June 2003; accepted 19 September 2003)

Focused surface-acoustic waves (SAWs) provide a way to reach intense acoustic fields for electro- and optoacoustic applications on semiconductors. We have investigated the focusing of SAWs by interdigital transducers (IDTs) deposited on (100)-oriented GaAs substrates. The focusing IDTs have curved fingers designed to account for the acoustic anisotropy of the substrate. Different factors that affect focusing, such as the aperture angle and the configuration of the IDT fingers, were systematically addressed. We show that the focusing performance can be considerably improved by appropriate choice of the IDT metal pads, which, under appropriate conditions, create an acoustic waveguide within the IDT. We demonstrate the generation of narrow (full width at half maximum of approx 15 μm), high-frequency (0.5 GHz), continuous SAW beams with vertical displacement as high as 4 nm collimated over distances that exceed 100 μm. © *2003 American Institute of Physics.* [DOI: 10.1063/1.1625419]

I. INTRODUCTION

Surface-acoustic waves (SAWs) are elastic vibrations that propagate on a free surface.[1–3] These waves generate spatially modulated mechanical displacement (the strain field) and, in the case of piezoelectric materials, also a piezoelectric field on the propagating surface. SAWs are particularly interesting in piezoelectric materials, where they can be efficiently generated through the inverse piezoelectric effect by means of interdigital transducers (IDTs) deposited on the materials surface. SAWs based on piezoelectric insulators have been used in a large range of applications in electronic signal processing and optoelectronics.

The III–V semiconductors, in particular GaAs, are interesting materials for SAW applications. Their piezoelectricity allows the electrical generation of SAW by IDTs, which can be fabricated using the well established technology for optoelectronic devices. While the initial SAW applications mainly included electronic signal processing devices based on strong piezoelectric materials, nowadays several alternative applications have been proposed that explore modulation of the optical properties and the acoustically induced transport of carriers by the SAW fields in semiconductors.[4,5] There has been renewed interest in SAWs since the demonstration that they can be applied to dynamically modulate the electronic properties of GaAs-based low-dimensional semiconductor structures like photonic crystals,[6] microresonators,[7,8] quantum wells,[9–11] quantum wires,[12] and quantum dots.[13] The traveling SAW fields in these structures have been used to transport electron-hole pairs[9,12,14] and spin excitation.[15]

Many of the applications mentioned above require a strong SAW beam concentrated on a small area of the sample surface. Such beams are normally difficult to generate by conventional IDTs deposited on GaAs due to the weak piezoelectric coupling of the material. One approach by which to produce strong SAW fields consists of using IDTs designed to generate a focused SAW beam.[16] Over the past few years, many reports have addressed the focusing mechanism in strong piezoelectric materials like $LiNbO_3$.[16–23] As in conventional optics, focusing in an acoustically isotropic medium can be achieved by shaping the fingers of the IDT in the form of an arc of the circumference.[19] The propagation properties of SAWs, however, are normally strongly anisotropic, thus requiring a more complicated IDT design. The best focusing performance is obtained when the group velocity of the SAW beam generated at each section of the IDT is directed radially towards the point of focus. The last condition is satisfied when the IDT fingers follow lines of the constant group velocity.[19–21]

In contrast to $LiNbO_3$, very few experimental investigations have addressed the focusing of SAW on GaAs substrates.[24–27] Most of these experiments were performed using transducers with fingers in the form of circumferences or of circumference segments, which do not take into account the material anisotropy. The influence of the acoustic anisotropy on the IDT performance has not been considered in these studies. Also, a quantitative study of the spatial profile of focused beams as well as of the effects of the IDT fingers on SAW propagation is still missing.

In this article, we present a detailed investigation of the concentration of SAW beams in GaAs using focusing IDTs. We start by reviewing important aspects related to the acoustic anisotropy in this material and how they can be taken into account in the design of focusing IDTs (Sec. II). These results are then applied to the fabrication of single (i.e., with two metal fingers per period) and double-finger (sometimes also called split-finger) IDTs (i.e., with four metal fingers per period) with operation frequencies of 1 and 0.5 GHz, respectively. We demonstrate that these devices can produce focused SAW beams with minimum full width at half maximum (FWHM) of less than three SAW wavelengths. We found that the focusing properties depend not only on the

[a]Author to whom correspondence should be addressed; electronic mail: mmlimajr@pdi-berlin.de

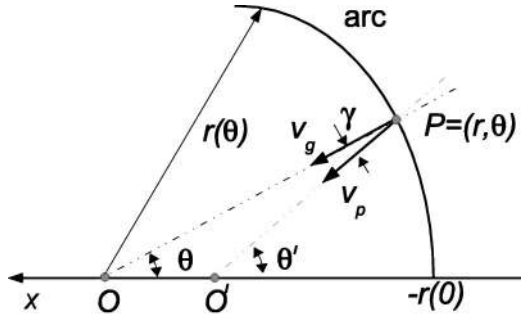

FIG. 1. Scheme of focusing of a surface-acoustic wave by an arc-shaped interdigital transducer finger. O denotes the focus position, θ and θ' are the propagation directions of the group (v_g) and phase velocity (v_p), respectively.

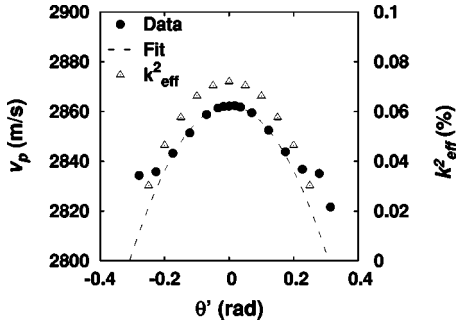

FIG. 2. Phase velocity v_p of the surface-acoustic wave (circles, from Ref. 30) and calculated effective electromechanical coupling k^2_{eff} (triangles) as a function of the deviation angle θ' from the $[0\bar{1}1]$ direction. The dashed line is a fit to the parabolic dispersion given by Eq. (1).

aperture angle of the transducer, but also on whether the IDT is of single-finger or double-finger type for the same finger shape. Much better performance is observed in the latter. This is attributed to the strong Bragg reflections of the acoustic wave on the metal fingers of the single-finger IDTs,[28] which considerably alter the angular dependence of the SAW phase velocity and scatter the SAW within the IDT into bulk modes. We show furthermore that under appropriate conditions the IDT pads play a fundamental role in the focusing characteristics by waveguiding the SAW beam within the transducers. This effect is particularly important in small aperture IDTs, where it can be used to correct diffraction effects and to produce SAW beams with waists considerably smaller than those predicted by diffraction theory.

II. FOCUSING IDTS

The SAW modes considered here are elastic vibrations with wave vector k_{SAW} forming a small angle θ' with the $[0\bar{1}1]$ direction of the (100) GaAs surface. These modes are superpositions of the longitudinal (L), the fast (T_1), and the slow (T_2) bulk transverse modes with the same wave vector k_{SAW}. In general, these waves have a displacement field with non-vanishing components along the $x=[0\bar{1}1]$, $y=[011]$, and $z=[100]$ directions, which satisfy the stress-free boundary condition in the surface plane. For propagation exactly along the x direction, the y component vanishes. In this case, the elastic mode becomes a true Rayleigh surface wave polarized in the xz plane. For other wave vector directions, (i.e., $\theta' \neq 0$), surface vibration turns into a leaky pseudosurface mode, which can be described as a pure Rayleigh mode coupled to the slow transverse T_2 bulk mode.[29] Attenuation of this pseudo-SAW mode (which will hereafter be denoted simply as SAW) is related to the fact that the velocity of the Rayleigh wave in GaAs lies above that of the T_2 bulk mode. The attenuation values depend on the wave vector angle θ' relative to the x direction, and reach a maximum of about 0.01 dB/λ_{SAW} for $\theta=0.14$ rad.[29]

The focusing of SAWs using curved IDTs is performed by the superposition of SAW modes with different propagation angles. In order to focus the SAW beam at the origin O (see Fig. 1), the beam generated by the IDT fingers at a position $P=(r,\theta)$ has to propagate with a group velocity directed along the line $\overline{OP}$, where the angle θ is used to describe the group velocity direction. This condition is satisfied if the shape of the IDT fingers coincides with the wave fronts emanating from a point source at O.[19,20] In order to calculate the geometric shape of the fingers, it is important to take into account the fact that the SAW propagation properties are strongly anisotropic in GaAs. For small deviation angles θ', the anisotropy in the phase velocity v_p can be described in terms of the anisotropy parameter a defined according to[2,16,18]

$$v_p(k_{\text{SAW}},\theta')=v_{p_0}k_{\text{SAW}}(1+a\theta'^2), \tag{1}$$

where v_{p_0} is the phase velocity for propagation along $[0\bar{1}1]$ (i.e., for $\theta'=0$). The anisotropy leads to a steering angle γ between the group and the phase velocity (cf. Fig. 1) given by

$$\gamma(\theta')=\tan^{-1}\frac{2a\theta'}{(1+a\theta'^2)}\sim 2a\theta', \tag{2}$$

where the approximation on the right-hand side applies when $a\theta'^2 \ll 1$. Using the previous expressions, it can be shown that the wave fronts leading to group velocities directing radially toward O follow the curve given by

$$r(\theta)=r(0)\exp\left[\frac{a}{1+2a}\theta^2\right]\sim r(0)\left[1+\frac{a}{1+2a}\theta^2\right], \tag{3}$$

with

$$\theta=(1+2a)\theta'. \tag{4}$$

Equation (3) yields a parabolic angular dependence of the radius r for small angles θ.[21]

In order to determine the anisotropy parameter a, we have used high precision data for the angular dependence of the SAW velocity reported for GaAs wafers in Ref. 30. The data, which are reproduced in Fig. 2 (circles), can be fitted well with a parabola [cf. Eq. (1)] in the angular interval $-0.1<\theta'<0.1$ rad ($-5.7°<\theta'<5.7°$), yielding anisotropy parameter $a=-0.229\pm0.02$ and phase velocity $v_{p_0}=2862.3$ m/s (dashed line). The parameter a determined above agrees very well with the value of 0.228 reported in

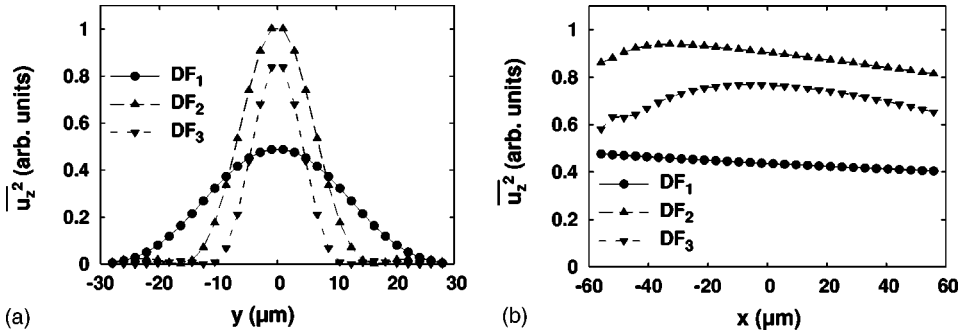

FIG. 3. Simulation of the square of the vertical displacement field averaged over time ($\overline{u_z^2}$) induced by a surface-acoustic wave along the directions (a) perpendicular (y direction) and (b) parallel (x direction) to the interdigital transducer axis, respectively. The dimension parameters for double-finger IDTs DF_1, DF_2, and DF_3 are summarized in Table I. The acoustic intensities are normalized to that of DF_2 at point $(x,y)=(0,0)$. The calculations were performed for $\lambda_{SAW}=5.6$ μm following the procedure outlined in Ref. 18.

Ref. 31, but is significantly lower than the one reported in Ref. 2. For calculation of the IDT fingers, we have used a value of $a=0.22$.

The deviations from parabolic behavior increase significantly for $|\theta'|>0.2$ rad. Taking into account Eq. (4), the maximum aperture angle ϕ, for which the parabolic approximation applies, becomes $\phi=2(1+2a)\theta'_{max}=0.22$ rad.

In order to determine the spatial distribution of the SAW fields in focusing IDTs, we have performed numerical calculations of the field intensity near the focus. The calculations were based on the Huygens principle following the procedure outlined in Ref. 18. According to the latter, each period of the IDT is viewed as a collection of SAW point emitters distributed along the IDT fingers. The SAW amplitude is obtained by integrating the contributions from all the emitters in the IDT. The calculations take into account the intrinsic anisotropy of the GaAs substrate, but neglect the dependence of the SAW attenuation on the propagation direction. However, they include the effects of the angular dependence of the electromechanical coupling coefficient, which controls the SAW generation efficiency. To that end, we have assumed the coupling coefficient k_{eff}^2 is proportional to the relative difference between the propagation velocity on the free and on the short-circuited surface. The calculated angular dependence of k_{eff}^2 is displayed by triangles in Fig. 2; note that, in agreement with Ref. 27, the coupling decreases with the deviation angle θ'. Together with deviation from the parabolic behavior mentioned above, the decrease in k_{eff}^2 imposes an upper limit on the maximum usable IDT aperture ϕ.

Figures 3(a) and 3(b) display simulation profiles of the square of the surface displacement field averaged over time ($\overline{u_z^2}$) along the directions perpendicular (y direction) and parallel (x direction) to the IDT axis. The calculations were performed for IDTs with emission wavelength $\lambda_{SAW}=5.6$ μm and angular aperture ϕ of 0.1 (DF_1), 0.2 (DF_2), and 0.3 rad (DF_3). Note that the two first apertures are within the limit of validity of the parabolic approximation, while the third one is beyond the limit. The length (l_{IDT}) as well as the minimum (w_{min}) and maximum (w_{max}) apertures of the IDTs are listed in Table I. The origin $(x,y)=0$ of the plots corresponds to point O defined in Fig. 1. To allow quantitative comparison between transducers, the vertical scales are normalized to $\overline{u_z^2}$ of IDT DF_2 at the origin.

The dependence of $\overline{u_z^2}$ along the line of focus (y direction) reproduces well the $\mathrm{sinc}^2\{k_{SAW}\phi/[2(1+2a)y]\}$ dependence expected from diffraction theory, where $\mathrm{sinc}(\eta)=\sin(\eta)/\eta$.[16,18] We verified that the correction due to the angular dependence of k_{eff} reduces the maximum intensity of

TABLE I. Summary of the parameters of the interdigital transducers used in this work. The properties displayed are the wavelength (λ_{SAW}) and the frequency (f_{SAW}), the aperture angle (ϕ), minimum (w_{min}) and maximum (w_{max}) apertures, length (l_{IDT}), and the area (A_{IDT}) of the IDTs. The last three fields on the right show the calculated ($w_b^{(c)}$) and measured ($w_b^{(m)}$) beam waists, and the effective rf-power coupling parameter Δs_{11}. IDTs labeled DF and SF indicate double- and single-finger structures, and subscripts L, 1, 2, and 3 denote linear IDTs and focusing IDTs with aperture angles ϕ of 0.1, 0.2, and 0.3 rad, respectively.

	IDT	ϕ (rad)	w_{min} (μm)	w_{max} (μm)	l_{IDT} (μm)	A_{IDT} (10^5 μm^2)	$w_b^{(c)}$ (μm)	$w_b^{(m)}$ (μm)	Δs_{11}
Set 1	DF_L	⋯	130	120	1960	2.35	⋯	⋯	0.38
$\lambda_{SAW}=5.6$ μm	DF_1	0.1	18	147	1330	1.07	63	35	0.24
$f_{SAW}=510$ MHz	DF_2	0.2	18	238	1120	1.41	31	26	0.22
	DF_3	0.3	24	273	840	1.23	21	24	0.13
Set 2	SF_L	⋯	64	60	560	0.34	⋯	⋯	0.71
$\lambda_{SAW}=2.8$ μm	SF_1	0.1	18	147	1330	1.07	31	24	0.43
$f_{SAW}=1.02$ GHz	SF_2	0.2	18	238	1120	1.41	16	19	0.18
	SF_3	0.3	24	273	840	1.23	10	21	0.13

$\overline{u_z^2}$ without appreciably changing its shape. The beam waist at the focus position, defined as twice the distance between the peak and the first zero of sinc, is given by[16,18,21]

$$w_b = 2\lambda_{SAW}(1+2a)/\phi. \quad (5)$$

In agreement with the last expression, the beam waists in Fig. 3(a) are inversely proportional to ϕ. The $\overline{u_z^2}$ profiles show a weak dependence on the distance along the IDT axis [Fig. 3(b)], thus indicating a large depth of focus. Finally, note that the maximum of $\overline{u_z^2}$ shifts toward the IDT as the aperture angle ϕ decreases. This is attributed to the increasing role of diffraction in narrow aperture IDTs.[18]

III. EXPERIMENT

A. IDT fabrication

The IDTs investigated here, which are listed in Table I, were fabricated on undoped (100) GaAs wafers with the IDT axis aligned along the $[0\bar{1}1]$ surface direction. In order to investigate focusing effects, two sets of focusing IDTs with aperture angles ϕ of 0.1, 0.2, and 0.3 rad were fabricated. Set 1 consists of double-finger IDTs designed for an operating wavelength of $\lambda_{SAW}=5.6\ \mu$m and frequency $f_{SAW}=510$ MHz. Within this set, the width and the spacing between two consecutive metal fingers corresponds to $\lambda_{SAW}/4$. The shape of the mth metal finger in these IDTs is given by Eq. (3) with $r(0)=m\lambda_{SAW}/4$. Set 2 is composed of single-finger IDTs [i.e., $r(0)=m\lambda_{SAW}/2$] for the generation of SAWs with wavelength $\lambda_{SAW}=2.8\ \mu$m (operating frequency of approx 1.02 GHz). Each set also includes a linear IDT. The width and spacing of the metal fingers are the same in sets 1 and 2. Note that the dimensions of the focusing IDTs are the same for both sets.

The IDT fabrication process employed contact photolithography followed by a lift-off metallization process. In contact lithography, the dimensions of the IDT structures are defined by a chromium lithographic mask, which was fabricated by electron-beam lithography. The nominal tolerance of the structures on the mask was ± 0.1 nm. The metal fingers in the focusing transducers were designed as small linear segments, following the parabolic shape given by Eq. (3). A large number of segments per finger (50) was used in order to keep the maximum length of the individual segments below one and two λ_{SAW} in the transducers of sets 1 and 2, respectively. The metallization film consists of a 10 nm thick Ti layer followed by a 40 nm Al layer and a second 10 nm Ti layer.

B. Measurements of the SAW field

The IDTs were excited by applying a radio-frequency (rf) power to its terminals. We will specify the power levels in terms of the nominal rf power P_{rf} supplied by the microwave generator. In order to determine the actual acoustic power, the rf reflection parameters were also measured by a network analyzer.

The measurements of SAW vertical displacement (u_z) were performed using a Michelson interferometer, which can detect vertical displacements a fraction of an angström. The interferometer operates using a single-mode laser source with a wavelength of 532 nm, which is focused to an approx 1 μm wide spot on the sample surface using a 50× objective. In order to check the spatial resolution of the interferometer, measurements of the SAW amplitude were also performed using a 100× objective. No difference was observed between the two cases, thus indicating that the SAW amplitudes are not limited by the spatial resolution of the measurement setup. Two-dimensional profiles of SAW vertical displacement u_z were obtained by scanning the laser beam over an area up to $100\times100\ \mu m^2$ on the sample surface. The output of the interferometer is detected by a fast photodiode (frequency response of 2 GHz). The amplitude of the diode signal, measured using a spectrum analyzer, is proportional to the time-averaged value $\overline{u_z^2}$. Phase sensitive measurements were performed by mixing the diode signal with the rf signal used to drive the IDT. The signal detected in this case is proportional to u_z.

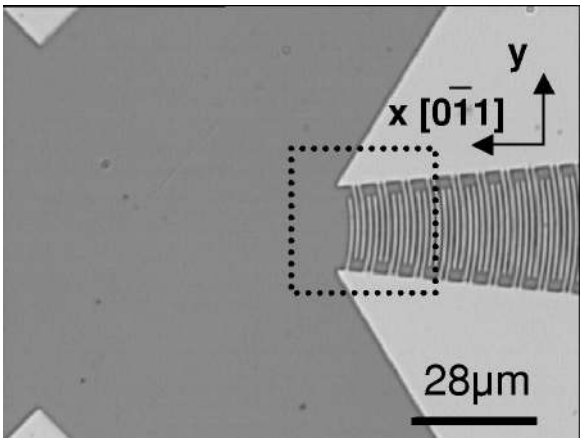

FIG. 4. Optical micrograph of the aperture output of a double-finger focusing transducer (DF_2 in Table I). The curved fingers are designed to follow the group velocity curves. The two triangles at the upper and lower left corners indicate the origin O (cf. Fig 1). The dotted rectangle indicates the area scanned in the interferometry measurement shown in Fig. 5.

IV. RESULTS

A. Beam profiles

Figure 4 shows an optical micrograph of the output aperture of transducer DF_2. The structure with curved double fingers, which follow the group velocity isotherms, can be observed. The two triangles in the left-hand corners point towards the origin O, which lies on the IDT axis.

Figure 5 shows profiles of u_z recorded on IDT DF_2 for a fixed phase of the SAW, and for excitation power $P_{rf}=10$ mW. These profiles were measured within the area indicated by the rectangle in Fig. 4, which is partially located within the IDT. The wave fronts of constant phase are very well defined and do not change as one goes from the region inside to the outside the transducer. Note, in addition, that the x position of the side lobes centered at $|y|\sim 15\ \mu$m, which correspond to the secondary maxima in the sinc function, coincides with that of the main lobe at $y=0$, thus indicating an almost flat wave front. Similar results were obtained for all double-finger transducers.

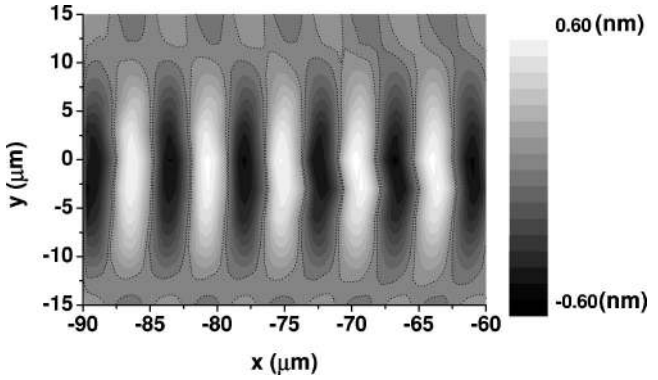

FIG. 5. Vertical displacement (u_z) measured by interferometry on double-finger interdigital transducer DF_2 (powered with $P_{rf}=10$ mW) in the area indicated in Fig. 4.

Figure 6 displays a spatial profile of $\overline{u_z^2}$ recorded over a large area in front of DF_1 under excitation with $P_{rf}=10$ mW. Figure 7 shows in a linear plot the integrated power flux across the beam cross section, defined as $I_x=\int_{-\infty}^{\infty}\overline{u_z^2}(x,y)dy$ as well as the beam waist as a function of the x position. It is interesting to note that the maximum intensity of $\overline{u_z^2}$ (and the minimum beam waist) of the beam is not located at the nominal focus [corresponding to $(x,y)=(0,0)$], but that the intensity increases (and the beam waist decreases) as one moves towards the edge of the IDT fingers (the IDT fingers are located at $x<-150$ μm). The FWHM at this position is only 15 μm, i.e., less than three times the SAW wavelength.

The small reduction in the maximum intensity of $\overline{u_z^2}$ with an increase in x is consistent with the large depth of focus predicted for DF_1 in Fig. 3(b). Note that the beam waist increases only 5% over the first 50 μm (approx 9 λ_{SAW}) from the IDT. The large amplitude and the good collimation over distances exceeding 100 μm make the focused SAW beam an ideal channel for acoustically induced transport. Furthermore, the SAW beam propagates for more than $150\lambda_{SAW}$ (approx 900 μm) without substantial attenuation. For distances that exceed 1000 μm, slight attenuation is observed.

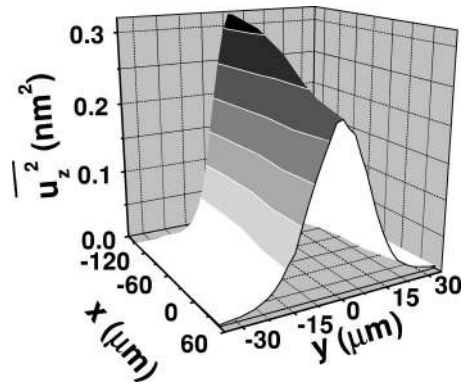

FIG. 6. Two-dimensional profile of the square of the vertical displacement field averaged over time ($\overline{u_z^2}$) measured in front of double-finger interdigital transducer DF_1 (powered with $P_{rf}=10$ mW). The position $(x,y)=(0,0)$ corresponds to the origin O (cf. Fig. 1).

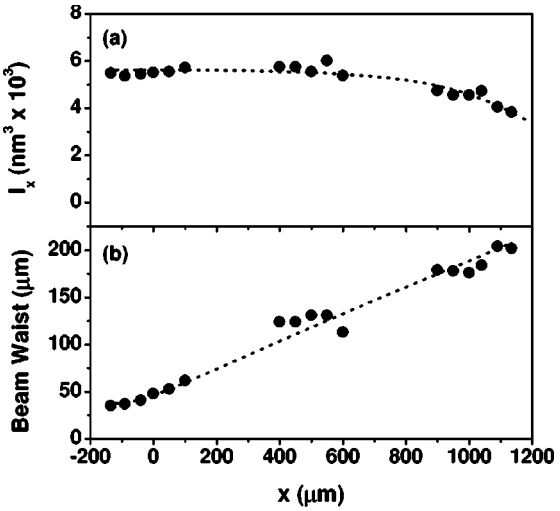

FIG. 7. (a) Integrated power flux $I_x=\int_{-\infty}^{\infty}\overline{u_z^2}(x,y)dy$ through the beam cross section and (b) beam waist w_b as a function of the distance from the focus for double-finger interdigital transducer DF_1. The position $x=0$ corresponds to the origin O.

The dependence of the focusing performance on the aperture angle is illustrated in Fig. 8, which shows cross sections of $\overline{u_z^2}$ measured along y in front of different focusing IDTs. The corresponding profile of a linear transducer DF_L is also shown for comparison. In all cases, the IDTs were excited with the same rf power $P_{rf}=10$ mW. In set 1, the $\overline{u_z^2}$ profiles narrows when ϕ increases from 0.1 to 0.2 rad, but a further increase to 0.3 rad leads to no significant reduction in beam waist. For IDTs with $\phi>0.2$ rad, the real dispersion [instead of the simplified parabolic approximation of Eq. (1)] has to be used to calculate the finger shape. We note, how-

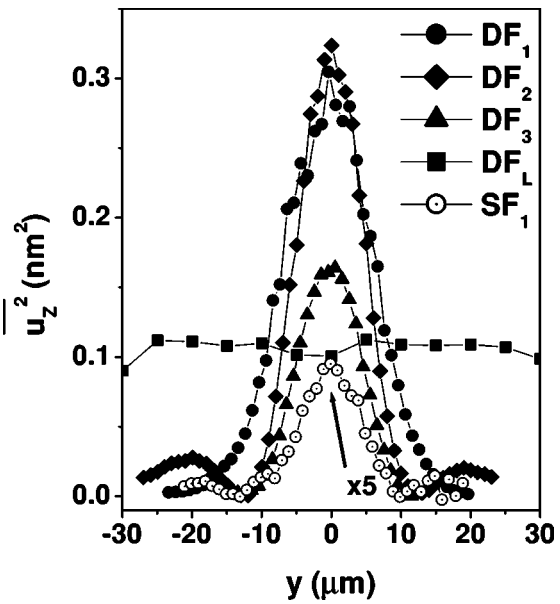

FIG. 8. Profile of the square of the vertical displacement field averaged over time ($\overline{u_z^2}$) along the beam cross section measured by interferometry in front of different focusing interdigital transducers of set 1. The profile for single-finger interdigital transducer SF_1 is also displayed for comparison.

ever, that since k_{eff} considerably decreases for $\phi > 0.2$ rad, only minor improvements are expected for larger ϕ.

Due to the lower operating wavelength, the IDTs of set 2 are expected to have a beam waist (w_b) equal to half that of set 1. Such behavior, however, is not observed in the experimental data. Moreover, in this set, no systematic dependence of w_b on ϕ was observed (cf. Table I), which is again at odds with the calculated results. Reasons for the bad focusing performance of the single-finger IDTs will be discussed in Sec. IV B.

The measured waists $w_b^{(m)}$, obtained by fitting the experimental data to the sinc^2 function defined in Sec. II A, are compared to the predictions $w_b^{(c)}$ of Sec. II A in Table I. In the case of double-finger IDTs, the calculations agree reasonably well with the experimental results for IDTs with large aperture angles. For $\phi = 0.1$ rad (see the data for DF_1), however, the measured waist is considerably smaller than the predicted one. The reason for the discrepancy between the measured and calculated waists in this case is attributed to the waveguiding effect introduced by the IDT pads. Metallization in the pad region leads to a difference in SAW velocity in the finger area ($v_{\text{SAW},f}$) and on the contact pads ($v_{\text{SAW},p}$) (see Fig. 4). Following the procedure described in Ref. 8 and assuming that the metallization consists of a single Al layer with an effective thickness of 60 nm, we calculate that, while $v_{\text{SAW},f}$ is essentially equal to the SAW velocity on the bare substrate, $v_{\text{SAW},p}$ is a factor of $n_v = 1.0032$ larger. The higher velocity in the pad region leads to confinement of the SAW mode in the finger region, thus reducing spreading of the beam by diffraction. In fact, by using simple arguments of geometric optics, we estimate from n_v an angle of total reflection of $\arcsin(n_v) = 85.4°$. The same model yields exponential decay of the SAW intensity in the pad region with a characteristic decay length of $\lambda_{\text{SAW}}/[4\pi\sqrt{(1-n_v^2)}] \sim \lambda_{\text{SAW}}$.[2,32] It is interesting to note that the FWHM of the SAW profiles for DF_1 and DF_2 in Fig. 8 is very similar to the IDT output aperture of 18 μm (as illustrated in Fig. 4, the aperture is slightly larger than the minimum width for overlapping of the fingers $w_{\min}$ listed in Table I).

In order to demonstrate the waveguiding effect produced by the fingers, we employed the IDT configuration with two focusing IDTs (of DF_1 type), shown in the inset of Fig. 9. The IDT on the right works as a source of a wide diverging SAW beam (beam waist of more than 150 μm), which is subsequently refocused by the IDT on the left. The latter was kept under open-circuit conditions. The squares and dots in Fig. 9 represent cross sections of $\overline{u_z^2}$ measured along lines A and B shown in the inset. Along line B, the beam waist reduces to values comparable to those displayed for DF_1 in Fig. 8. Narrowing of the SAW beam could also be due to strong SAW absorption in the metal pads. We checked this possibility by short circuiting the IDT on the right during measurement in order to simulate conditions under a metallized surface. No appreciable change in transmission was observed, thus eliminating absorption effects and providing evidence of the role of metallization pads as cladding regions.

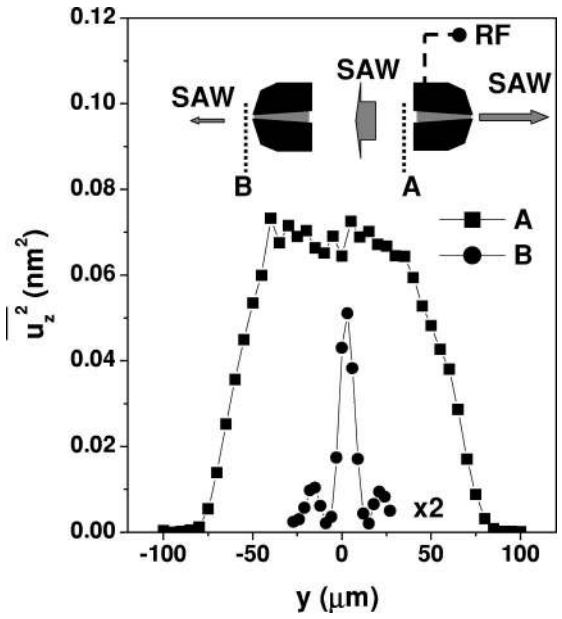

FIG. 9. Cross sections of the square of the vertical displacement field averaged over time ($\overline{u_z^2}$) measured along lines A and B in the configuration displayed in the inset. The distance between these two lines is 2.4 mm. The interdigital transducer on the right is used as a surface-acoustic wave generator and the IDT on the left as a passive SAW concentrator (both IDTs are double finger of DF_1 type). The IDT on the right was powered with $P_{\text{rf}} = 10$ mW while the one on the left was kept under open-circuit conditions.

B. Focusing efficiency

The performance of focusing IDTs is judged not only by the minimum beam waist, but also by the intensity of the SAW beam it can produce. As will be demonstrated here in Sec. IV B, a analysis of the beam intensity also allows us to determine the mechanisms that limit the focusing performance of the devices.

The measurements in Fig. 8 were performed by applying the same nominal rf power of $P_{\text{rf}} = 10$ mW to the different IDTs. According to Fig. 8, the highest SAW amplitudes in set 1 were obtained for transducers DF_1 and DF_2. The superior capability of these IDTs to produce large SAW amplitudes compared to linear IDTs becomes even more evident if we take into account the fact that the conversion efficiency between electrical and acoustic powers is considerably smaller in focusing devices, since their design was not optimized to improve rf coupling. The electrical conversion efficiency is quantified by $\Delta s_{11} = s_{11}^{(f_{\text{SAW}})} - s_{11}^{(0)}$, where $s_{11}^{(f_{\text{SAW}})}$ and $s_{11}^{(0)}$ denote the rf-reflection coefficient at the SAW resonance frequency and outside it, respectively. Δs_{11} is listed for the different transducers in Table I. In general, Δs_{11} decreases with an increase in aperture angle. In set 1, the lower value of Δs_{11} of the focusing IDTs compared to the linear one is partially due to the smaller area.

The results described in the previous paragraph indicate that the SAW amplitude can be substantially increased by improving rf coupling to the IDT. In fact, we were able to double $\overline{u_z^2}$ of DF_2 by using a stub matching box. By applying a rf power of 250 mW, vertical displacements $|u_z|$ as large as 4 nm could be generated by this IDT.

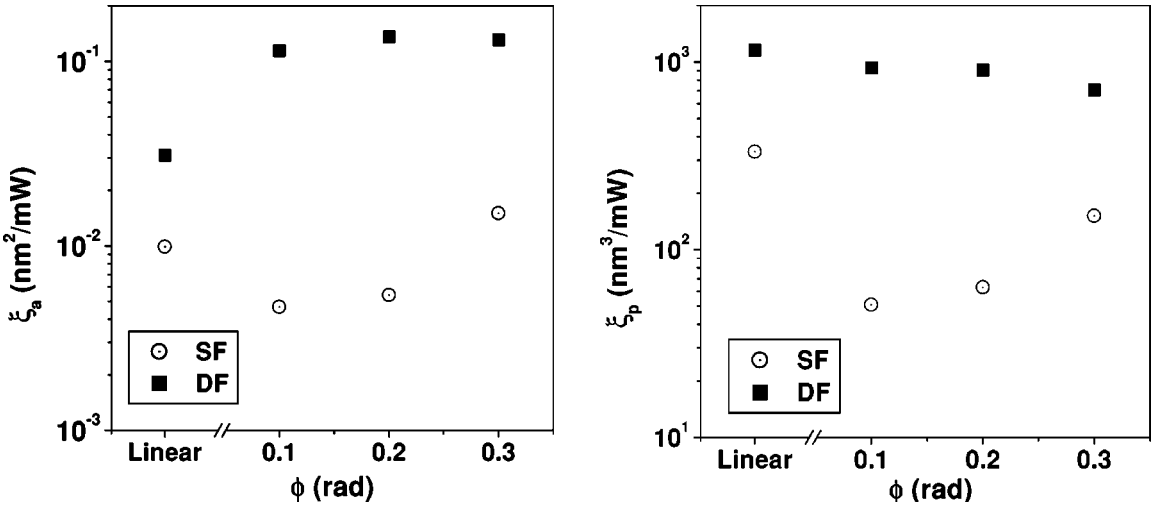

FIG. 10. Experimental results for the (a) amplitude (ξ_a) and (b) power efficiency (ξ_p) of the single-finger (SF) and double-finger (DF) interdigital transducers.

Figure 10(a) displays the normalized ratio $\xi_a = \overline{u_z^2}(y=0)/(\Delta s_{11} P_{\mathrm{rf}})$, which expresses the capability of the transducer to produce high SAW amplitude at the output of the IDT per unit of acoustic power. For the IDTs in the first set, ξ_a is approximately four times larger for the focusing IDTs than for the linear one. Likewise, the beam waist ξ_a saturates for apertures $\phi > 0.1$ rad for the IDTs in set 1 (cf. Table I).

In contrast, the single-finger IDTs (set 2) display much lower ξ_a. The reasons for such poor performance can be understood if one considers the total SAW flux that crosses the focus plane. The latter will be stated in terms of a power coefficient ξ_p defined as

$$\xi_p = \frac{f_{\mathrm{SAW}}}{1\ \mathrm{GHz}} \frac{1}{\Delta s_{11} P_{\mathrm{rf}}} \int_{-\infty}^{\infty} \overline{u_z^2}(0,y)\, dy. \tag{6}$$

Since the aperture angles are very small for all IDTs, ξ_p is proportional to the fraction of rf power converted into a SAW mode, which subsequently propagates through the focus plane. Note that, contrary to ξ_a, this parameter also takes into account SAW loss due to conversion to bulk modes either during generation or during propagation to the focus plane. The frequency ratio $f_{\mathrm{SAW}}/(1\ \mathrm{GHz})$ accounts for the inverse dependence of $\overline{u_z^2}$ on frequency, thus allowing comparison of transducers with different operation frequencies. In set 1, ξ_p decreases with ϕ, thus indicating that either (i) a larger fraction of bulk-like acoustic modes is generated by the IDT fingers or (ii) the SAW is increasingly attenuated during propagation.

The values of ξ_p are significantly smaller in the IDTs of set 2. Except for the finger arrangement, the focusing IDTs in this set have the same dimensions as those in set 1. The small ξ_p's thus indicate that the reduction is due to mechanism (ii), i.e., to attenuation of the SAW during propagation. The high attenuation rates in set 2 are attributed to strong reflection of the SAW beam on the metal fingers. In fact, it is well known that the metal fingers in the single-finger IDTs act as an efficient first-order Bragg reflection grating for the SAW, since their separation corresponds exactly to $\lambda_{\mathrm{SAW}}/2$. The strong Bragg reflections turn these IDTs into a standing wave cavity for the SAW beam with high acoustic amplitude inside the transducer. The multiple reflections in the single-finger IDTs increase scattering of the SAW into bulk modes, thus reducing the efficiency of ξ_a and ξ_p (cf. Fig. 10). The reflection effects are minimized in the double-finger configuration, where the metal grating is changed into a second-order grating at the SAW wavelength by doubling the number of fingers per period.

The cavity effect becomes apparent by comparing the SAW amplitudes at the center and at the output aperture of the transducers. For the double-finger focusing transducers, $\overline{u_z^2}$ increases continuously as one goes from the wide to the narrow aperture. In contrast, for the single-finger structures $\overline{u_z^2}$ always reaches its maximum inside the IDT. The effect is particularly strong for the linear transducer SF_L, where the $\overline{u_z^2}$ at the center of the finger region is approximately 30 times larger than that at the output ends.

The cavity effect has also consequences for the focusing performance, since it is expected to change the angular dependence of the SAW velocity and, thus, the effective anisotropy parameter a. Furthermore, due to the strong reflections and scattering in bulk modes, only the fingers close to the narrow IDT output aperture contribute to the SAW emitted field. In the design employed here, the effective emission area becomes very small, thus leading to the low SAW intensities of the focusing single-finger structures. In fact, the increase in efficiency of the single-finger IDTs with an increase in aperture angle ϕ can be accounted for by the increase in effective emission area. Better performance is then expected by (i) increasing the length and (ii) reducing the number of fingers.

V. CONCLUSIONS

In summary, we have investigated the concentration of SAW beams in GaAs using focusing IDTs. Two focusing mechanisms were identified. The first is associated with the curved shape of the IDT fingers, which were designed to generate a SAW beam with group velocity directed towards

the focus point. In the design, it is important to take into account the acoustic anisotropy of the material. The latter, limits the maximum aperture angle ϕ of the focusing IDTs to values less than approx 0.2 rad due to (i) deviation of the relationship v_{SAW} versus angle from parabolic behavior, (ii) reduction of the SAW generation efficiency, and (iii) enhanced excitation of bulk modes for large ϕ values.

The second focusing mechanism is associated with the total reflection of the SAW at the interface between the finger region and the contact pads of the IDT, and it occurs when the SAW velocity in the latter exceeds that in the former region. This condition is achieved when Al is used as metallization layer for IDTs on GaAs. The pads act, in this case, as cladding regions for waveguiding of the SAW mode, thus confining the beam within the finger area. The waveguiding effect is particularly important for reducing diffraction effects in narrow aperture transducers, which leads to much smaller beams waists. This interesting concentration mechanism can be used to overcome some of the limitations that arise from the small aperture angles.

By combining the two mechanisms described above, the best focusing performance was obtained in double-finger IDTs with aperture angles of 0.1 and 0.2 rad. The performance of single-finger transducers is worse than that of their double-finger counterparts: we have identified the strong Bragg reflection of the SAW beam at the IDT fingers as the main cause of performance degradation. Finally, we have demonstrated excitation of 0.5 GHz SAWs with displacement amplitude of 4 nm for nominal rf power of 250 mW with a beam waist of 26 μm. The FWHM of the beam amounts to only 15 μm. The small divergence and waist of the focused beams together with the large depth of focus (around 9 λ_{SAW}) make them ideal transport channels for acoustically induced carrier transport in GaAs.

ACKNOWLEDGMENTS

The authors thank H. Grahn for comments and for critical reading of the manuscript as well as C. Flannery for making his experimental data on the GaAs acoustic dispersion available to them. The authors acknowledge the technical expertise of S. Krauss in the preparation of the samples for optical measurements. Support from the Deutsche Forschungsgemeinschaft (Project No. SA598/3-1) is gratefully acknowledged.

[1] R. M. White, Proc. IEEE **58**, 1238 (1970).
[2] A. A. Oliner, *Acoustic Surface Waves* (Springer, Berlin, 1994).
[3] D. Royer and E. Dieulesaint, *Elastic Waves in Solids* (Springer, Heidelberg, 2000).
[4] F. C. Jain and K. K. Bhattacharjee, Proc. SPIE **1347**, 614 (1990).
[5] M. J. Hoskins, H. Morkoç, and B. J. Hunsinger, Appl. Phys. Lett. **41**, 332 (1982).
[6] P. V. Santos, J. Appl. Phys. **89**, 5060 (2001).
[7] F. W. Beil, A. Wixforth, and R. H. Blick, Physica E **13**, 473 (2002).
[8] Y. Takagaki, E. Wiebicke, P. V. Santos, R. Hey, and K. H. Ploog, Semicond. Sci. Technol. **17**, 1008 (2002).
[9] C. Rocke, S. Zimmermann, A. Wixforth, J. P. Kotthaus, G. Böhm, and G. Weimann, Phys. Rev. Lett. **78**, 4099 (1997).
[10] P. V. Santos, M. Ramsteiner, and F. Jungnickel, Appl. Phys. Lett. **72**, 2099 (1998).
[11] T. Sogawa, P. V. Santos, S. K. Zhang, S. Eshlaghi, A. D. Wieck, and K. H. Ploog, Phys. Rev. B **63**, 121307(R) (2001).
[12] F. Alsina, P. V. Santos, H.-P. Schönherr, W. Seidel, K. H. Ploog, and R. Nötzel, Phys. Rev. B **66**, 165330 (2002).
[13] C. Bödefeld, A. Wixforth, J. Toivonen, M. Sopanen, and H. Lipsanen, Phys. Status Solidi B **224**, 703 (2001).
[14] F. Alsina, P. V. Santos, R. Hey, A. García-Cristóbal, and A. Cantarero, Phys. Rev. B **64**, 041304 (2001).
[15] T. Sogawa, P. V. Santos, S. K. Zhang, S. Eshlaghi, A. D. Wieck, and K. H. Ploog, Phys. Rev. Lett. **87**, 276601 (2001).
[16] M. G. Cohen, J. Appl. Phys. **38**, 3821 (1967).
[17] I. M. Mason and E. A. Ash, J. Appl. Phys. **42**, 5343 (1971).
[18] J. B. Green, G. S. Kino, and B. T. Khuri-Yakub, in *Proceedings of the 1980 IEEE Ultrasonic Symposium*, edited by B. R. McAvoy (IEEE, New York, 1980), pp. 65–73.
[19] Y. N. Borodii, I. M. Grankin, and Y. V. Nepochatykh, Sov. Phys. Acoust. **31**, 264 (1985).
[20] J. Z. Wilcox and R. E. Brooks, J. Appl. Phys. **58**, 1148 (1985).
[21] J. Z. Wilcox and R. E. Brooks, J. Appl. Phys. **58**, 1160 (1985).
[22] S. R. Fang, S. Y. Zhang, and Z. F. Lu, IEEE Trans. Ultrason. Ferroelectr. Freq. Control **36**, 178 (1989).
[23] H. E. Engan, T. Myrtveit, and J. O. Askautrud, Opt. Lett. **24**, 24 (1991).
[24] W. Sauer *et al.*, Appl. Phys. Lett. **75**, 1709 (1999).
[25] M. Streibl, H.-J. Kutschera, W. Sauer, and A. Wixforth, in *Proceedings of the 2000 IEEE Ultrasonics Symposium*, edited by S. C. Schneider, M. Levy, and B. R. McAvoy (IEEE, New York, 2000), pp. 205–208.
[26] C. Bödefeld, F. Beil, H.-J. Kutschera, M. Streibl, and A. Wixforth, 2001 Ultrasonic Symposium, 2001, p. 69.
[27] T. Hesjedal and G. Behme, Appl. Phys. Lett. **79**, 1054 (2001).
[28] A. J. De Vries, R. L. Miller, and T. J. Wojcik, in *Proceedings of the 1972 IEEE Ultrasonic Symposium*, edited by J. De Klerf (IEEE, New York, 1972), pp. 353–358.
[29] W. D. Hung, R. L. Miller, and B. J. Hunsinger, J. Appl. Phys. **60**, 3532 (1986).
[30] C. M. Flannery, E. Chilla, S. Semenov, and H.-J. Fröhlich, in *Proceedings of the 1999 IEEE Ultrasonic Symposium*, edited by S. C. Schneider, M. Levy, and B. K. McAvoy (IEEE, New York, 1999), pp. 501–504.
[31] W. D. Hung, Y. Kim, and F. M. Fliegel, J. Appl. Phys. **69**, 1936 (1991).
[32] H. Seidel and D. L. White, U.S. Patent No. 3,406,358 (filed 1968).